PREPRINT Mizuno, T. *Method of controlling a chemically-induced nuclear reaction in metal nanoparticles.* in *ICCF18 Conference*. July 2013. University of Missouri. Addendum with new data, November 2013.

# Method of controlling a chemically-induced nuclear reaction in metal nanoparticles

Tadahiko Mizuno
Hydrogen Engineering Application & Development Company
Three System Building 6 floor,
Kita-ku, North 12, West-4, 1-15, Sapporo 001-0012

## Abstract

A nuclear reaction can occur when metal nanoparticles are exposed to hydrogen isotopes in the gas phase. When hydrogen isotopes (light hydrogen and deuterium) enter the nanoparticles and are exposed to electron irradiation, the hydrogen reacts inside the lattice, producing energy. The reaction also produces neutrons, gamma rays and transmutations. Normally, electron irradiation does not produce anomalous heat or radiation. A reaction occurs when hydrogen acts as a heavy fermion (a heavy electron) inside metal nanoparticles below a certain particle size, allowing protons or deuterons to approach one another closely.

Usually, with deuterium, to cause a fusion reaction it is necessary to supply energy of $10^7$ K, or 1 keV per atom. With light hydrogen it is necessary to supply $1.5 \times 10^7$ K, for a reaction rate of $10^{-31}$. With a reactor system on a scale smaller than the sun, a significant fusion reaction does not occur. However, when heavy electrons enter the outer shell of a proton, the radius of the hydrogen atom becomes exponentially smaller with respect to the weight of the heavy electrons, bringing the protons closer together. When this happens, the probability of tunneling fusion increases exponentially.

The nuclear reaction can be controlled with this energy production method of bringing protons and heavy electrons together inside nanoparticles. This brings within reach the goal of developing a practical nanoparticle energy reactor.

## 1 Theory

### 1.1 Summary

A population of free electrons in 10 nm metal nanoparticles are subjected to strong forces by the metal atoms and by other electrons. This occurs when:

1. Hydrogen isotopes are injected into nanoparticles.

2. This causes the hydrogen density to rise, changing the nature of the nanoparticles, which increases the effective mass of electrons to a high level.
3. Heavy electrons combine with hydrogen nuclei to form atoms.
4. When heavy electrons become extranuclear electrons the electron orbital radius shrinks.
5. The distance between the nucleus and the heavy electron shrinks.
6. The probability of nuclear fusion between hydrogen atoms increases because of the tunneling effect.
7. When the mass of electrons doubles, the probability of fusion increases by 10 orders of magnitude.
8. The reaction causes heat.
9. The reaction may cause neutrons, helium and other reaction products.
10. Other elements that easily generate heavy electrons increase the fusion probability between heavy electrons and hydrogen nuclei include: alkali and alkaline-earth elements (such as Li, Na, K, Ca, and so on which have atomic structures similar to hydrogen). These elements enhance the electron transfer effect.

## 1.2 Calculating the tunneling effect

When a proton actually approaches $x = \delta$ (that is, the distance at which separate protons touch) then the electrostatic potential that repels protons from one another is overwhelmed by an attractive potential 5 orders of magnitude stronger. Therefore, the area $x \geqq \delta$ probability density function becomes $\phi 2 = 2\beta \cdot e - 2\beta x$ where fusion is likely to occur.

Where $\gamma$ is the probability of nuclear fusion:

$$\gamma = \int_{\delta}^{\infty} \psi^2 dx = \int_{\delta}^{\infty} 2\beta \cdot e^{-2\beta x} dx = - \left[ e^{-2\beta x} \right]_{\delta}^{\infty} = e^{-2\beta\delta}$$

$\therefore$ the probability of fusion $\gamma = e^{-2\beta\delta}$ (where $\beta = (2\pi / h) \cdot \{2m(U - E)\}^{1/2}$)

This is the probability of fusion between protons. Theoretically, it should allow the tunneling effect.

Here:

U: The electrostatic potential between two protons $= 1.15 \times 10^{-13}$J

E: The kinetic energy of a direct collision of protons, computed here for the center of the sun. That is, 15 million K $= 4 \times (3/2)kT = 1.24 \times 10^{-15}$J

Here, h: Planck's constant = $6.625 \times 10^{-34}$J・s

M: mass of a proton $= 1.7 \times 10^{-27}$kg

$\delta$: the necessary penetration distance of the proton $= 1.86 \times 10^{-13}$m

$\beta = (2\pi / h) \cdot \{2m(U - E)\}^{1/2} = 1.87 \times 10^{14}$

The resulting probability of fusion is:

$$\gamma = e^{-2\beta\delta} = 6.14\times10^{-31}$$

From the above, the probability that γ fusion will occur is obtained. The probability is very low, with fusion occurring once in every $10^{31}$ head-on collisions. There is an observable fusion reaction in the sun because there are so many collisions.

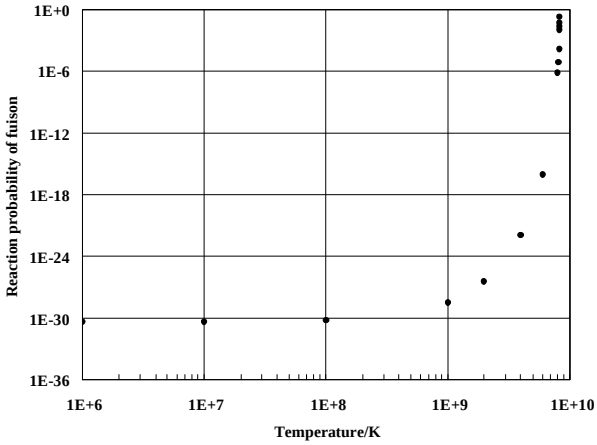


**Figure 1. Tunneling fusion effect dependence on proton temperature.**

Here is the calculation when the reaction occurs with heavy electrons. For example, with palladium nanoparticles, the effective mass of heavy electrons is increased by a factor of 2, and the tunneling effect rate increases by 10 orders of magnitude.

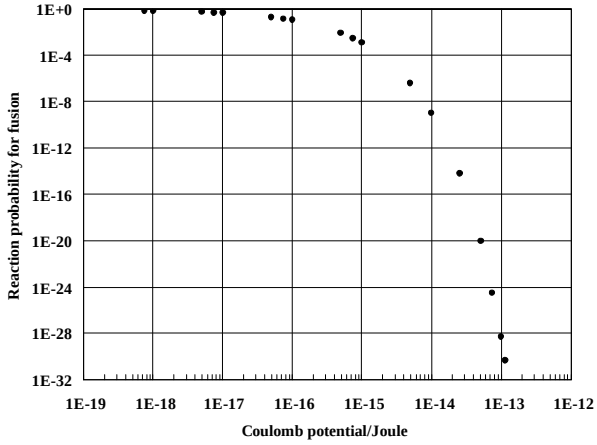


**Figure 2. Fusion probability dependence on proton separation potential.**

Here is an actual example of glow discharge with current density of 1 ~ 100 mA/cm$^2$. Every second, $6.24 \times 10^{18}$ hydrogen atoms are supplied to the metal surface. The total number of hydrogen atoms accumulating in the metal is equal to the average number of metal atoms in the nanoparticles. When the glow discharge continues long enough, nanoparticles form over the entire surface of the palladium.

Here is the calculation of the size of the effect assuming the entire surface of the metal has been converted to nanoparticles. The nanolayers are approximately 10 atoms thick, so there are approximately $10^{17}$ hydrogen atoms per centimeter of metal nanoparticles. Glow discharge electrolysis supplies the hydrogen atoms at a constant rate. The probability of the reaction is $10^{17} \times 10^{-20} = 10^{-2}/s/cm^2$. This translates to about 100 W of heat.

Normally, it is very difficult to sustain a stable nuclear reaction with hydrogen atoms. However, with this method it is not difficult, even though this method uses cheap, abundant materials.

Here is the calculation for hydrogen atoms. Heavy electrons enter the atomic orbitals of the hydrogen. The distance is determined by the electron mass of the nanoparticles. The heavy electrons cause the following reaction:

$$(p\ e^-_h) + H \rightarrow (pp\ e^-_h) + e\text{-}^*$$

$$\rightarrow 2D + \beta^+ + e^-_h + \nu_e + 0.164\ MeV$$

The reaction produces a deuteron, a positron and a meson. The heavy electron then returns to the nanoparticle lattice. If electrons are present it is possible the positron will produce a gamma ray. However, the probability of this is low.

$$\beta^+ + e^- \rightarrow 2\gamma + 1.022MeV$$

$^3$He can be produced, when the reaction forms a deuteron and a new heavy electron. A gamma ray is produced when this happens. The heavy electron returns to the nanoparticle.

$$^2D + (p\ e^-_h) \rightarrow {}^3He + \gamma + e^-_h + 5.493\ MeV$$

It is possible for the newly formed $^3$He, a heavy electron and a proton to undergo this reaction:

$$(p\ e^-_h) + {}^3He \rightarrow {}^4He + 2p + e^-_h + 12.860\ MeV$$

When all of these reactions occur in series, the total amount of energy produces is 26.218 MeV.

$$(p\ e^-_h) + 3H_2 \rightarrow 4He + e^-_h + 26.218\ MeV$$

With deuterium, a deuteron with a heavy electron forms, just as a proton pairs with a heavy electron starting with hydrogen.

$$(d\ e^-_h) + (D_2) \rightarrow [(dd\ e^-_h) + dee]^*$$

The reaction continues, producing fusion, which produces tritium, protons, $^3$He and neutrons. All of these reactions together produce 3.27 ~ 4.03 MeV of heat.

$$[(dd\ e^-_h) + dee]^* \rightarrow T + p + e^-_h + 4.03MeV$$

$$\rightarrow {}^3He + n + e^-_h + 3.27MeV$$

When Li is introduced into the nanoparticle environment, tritium and helium are produced by the following steps:

$^{6}Li + {}^{1}n \rightarrow {}^{4}He + {}^{3}H$

$^{7}Li + {}^{1}n \rightarrow {}^{4}He + {}^{3}H + {}^{1}n$

Since 92.5% of Li is $^{7}Li$, neutrons produce $^{4}He$ and $^{3}H$. This nuclear fusion reaction has been experimentally confirmed.

# 2 Method of Control

## 2.1 Gas

The reaction gases are hydrogen or deuterium. The gas purity is 99.99% for hydrogen ($H_2$), and 99.9% for deuterium (for D, or for $D_2$, 99.8%, HD, 0.2%).

## 2.2 Reactant

The reactant is commercial grade nickel wire, 0.1 to 1.0 mm thick, 99.9% purity.

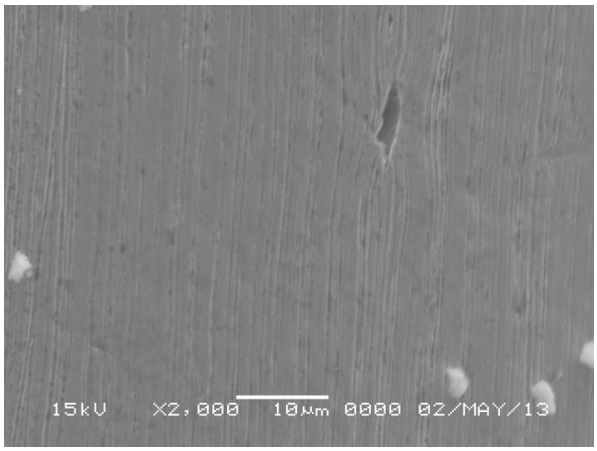


**Figure 3. A scanning electron micrograph (SEM) of the nickel wire before use.**

Figure 3 shows a scanning electron micrograph (SEM) (JSM, model 6060LV) of nickel wire before the test. The fine grooves on the surface are due to the processing in preparation for the test.

Other reactants include:

Commercial grade nickel plate, 0.3 ~ 1 mm thick, 99.9% purity.

Commercial grade nickel mesh made from 0.2 mm wire.

Commercial grade palladium wire, 0.1 ~ 1.0 mm thick, 99.9% pure.

Commercial grade palladium plate, 0.1 ~ 0.4 mm thick, 99.9% pure.

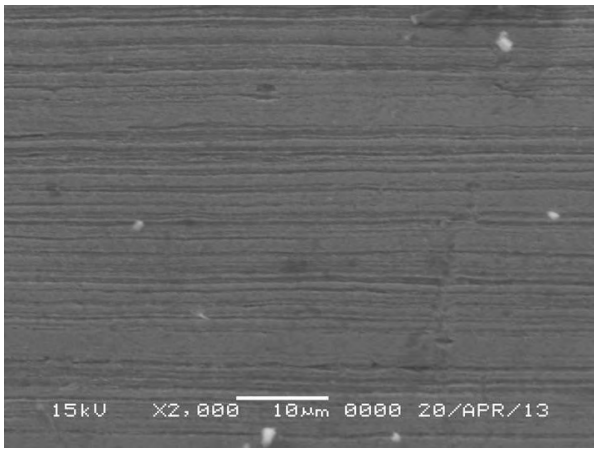


**Figure 4. SEM of the thin palladium wire before use.**

Figure 4 shows diameter 0.2 mm palladium wire. Like the nickel wire, it has fine grooves from processing.

**Counter-electrode**: With nickel wire the counter-electrode is either 1 mm diameter 30 mm long wire, or thinner 0.1 mm diameter, 1000 mm long wire, both wrapped in a spiral around a rod.

The shape is as shown in Fig. 5. The nickel wire is wrapped around an ICF70 copper connector, length 50 cm, thickness 1.6 mm in the copper portion, which is attached to a nickel tube, 20 cm long with an inner diameter of 3 mm. 50 mm of the tip is covered with an alumina insulating tube, 6 mm thick, inner diameter 4 mm. The nickel tube and alumina insulating tube are attached together with Torr Seal vacuum adhesive epoxy. The epoxy is allowed to dry and set for several days before the test to ensure it does not emit any gases. The nickel wire is wrapped as tightly as possible, as shown in the photograph. It is arranged so there are no protruding or pointed surfaces. Before use, the entire electrode assembly is washed in alcohol and acetone, in particular to eliminate contamination from fats and oils.

**Figure 5. The structure of the counter-electrode.**

Another type of counter-electrode used in this study consists of nickel wire 1 mm in diameter 300 mm long wrapped in a spiral.

Glow discharge serves two purposes in this experiment. It is used initially to create metallic nanoparticles on the surface of the counter-electrodes with direct electron irradiation. Later, as it continues, glow discharge loads the nanoparticles with hydrogen, causing a cold fusion reaction.

## 2.3 Shape

The smaller the nanoparticles in a sample are, the more effectively they absorb hydrogen, and the faster the reaction will occur. The effect works best with a particle size of 2 ~ 5 nm, where the number of atoms per particle is be $10^3$ ~ $10^4$.

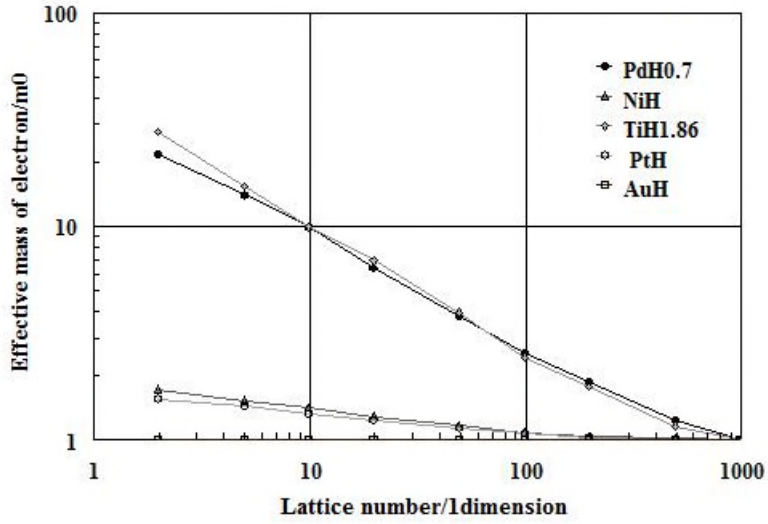


**Figure 6. Number of particles and mass of heavy electrons in nanoparticles.**

As shown in Fig. 6, when nanoparticles absorb large amounts of hydrogen, the particle size and number of atoms (horizontal axis), and the ratio of nanoparticles and electrons (vertical axis, where 1 is the ratio for electrons in bulk metal), the ratio decreases noticeably when the lattice number falls below 100, and as it approaches 1 (on the left) it increases by a factor of 10. This is most noticeable with palladium and titanium. With nickel when the lattice number is below 10 the effective mass increases about 50%. However, for gold, the effective mass does not increase because gold does not absorb hydrogen.

## 2.4 Reactors

Two reactors were used in this study, a small one and a large one.

A stainless steel reactor vessel is used for both. Grade 316 stainless steel is preferred. The vessels about as wide as they are tall, being cross-shaped with the gas inlet and window ports. Electrodes are introduced from the top, and there are a variety of connection terminals at the sides, including the gas inlet, pressure gauge and vacuum exhaust. The viewing window is made of Kovar glass. All connections are ICF flanges. The flange sizes are: top and base, 213 ICF; the middle portion flanges are 152 ICF; the front widow flange is 114 ICF; and the bottom mounting 70 ICF. The electrode connections are made through a 34 ICF flange. The gas inlet is made of ¼ Swagelok pipe and a ¼ Swagelok needle valve. The flange connections all use oxygen-free copper gaskets to prevent vacuum leaks.

In both reactors a nickel mesh is placed against the reactor wall, as shown in Fig. 12. This shields the steel reactor walls against stray plasma. The mesh is made of pure nickel and it is cleaned with alcohol and acetone, so when the plasma impinges on it, it releases less contamination than the bare cell wall would.

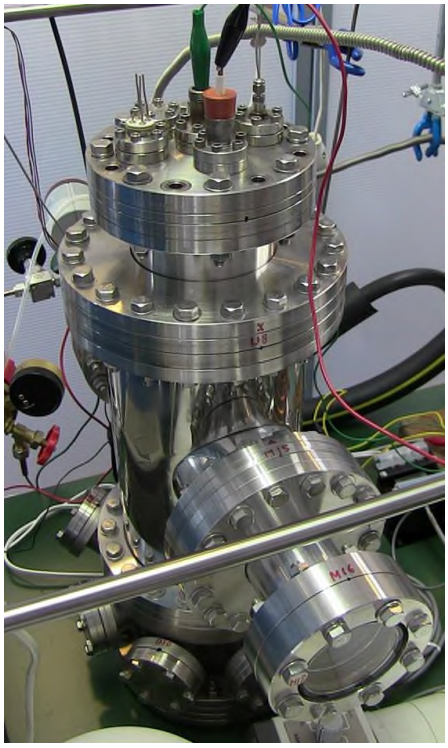

Figure 7. Large reactor vessel.

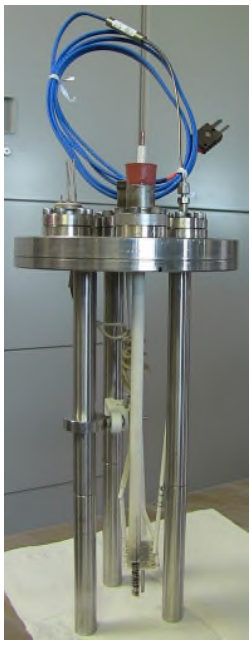

Figure 8. Large reactor lid and electrodes.

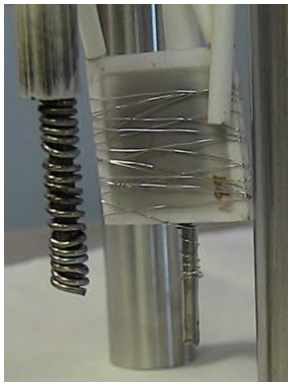

Figure 9. Large reactor electrodes.

## Description of large reactor and electrodes

A cross section of the large reactor is shown in Fig. 10. The reactor vessel is made from SUS316 stainless steel, with a volume of 15 L. It is 500 mm tall, and about 500 mm wide as well. It weighs 50 kg. The electrodes are shown in Fig. 9. The core of the electrode is a square alumina ceramic holder, 30 mm per side, 2 mm thick, with palladium wire wrapped around it. The wire is 0.2 mm thick, 1000 mm long, and is coiled around the ceramic holder about 15 times. The other electrode is made with 300 mm of palladium wire wrapped in a tight spiral around a palladium tube, which is 50 mm long, 3 mm in diameter. As noted, the entire assembly is washed in alcohol and acetone, and kept clean thereafter. Also as noted there was no trace of contamination from fats.

As shown in Fig. 8 the two electrodes enter the cell through the lid. Both are insulated. It is possible to change the polarity of the electrodes. The entire reactor vessel is grounded for safety.

The temperature of the electrodes is measured directly with a thermocouple (shown in the upper right pin in Fig. 10). This is a K-type thermocouple, 1.6 mm diameter, 300 mm long, in a stainless steel jacket. It touches the surface of the electrode wrapped around the ceramic holder. There are two other thermocouples in contact with the outside surface of the reactor: T5, in the middle of the cell, and T6 at the base. As shown in Fig. 9, there is a Kovar glass window on the side of the reactor vessel, which allows direct observation of the glow discharge conditions. As shown on the right

side of the figure there is a valve, pressure gauge (vacuum gauge), a gas inlet tube, and a vacuum tube. The pressure gauge is an MKS Baratron, equipped with an absolute pressure transducer (model 622A). The MKS power supply and digital readouts are model PDR-C-1C/2C. The resistance heater is used for the initial heat treatment of the electrodes, and also to calibrate the cell for calorimetry.

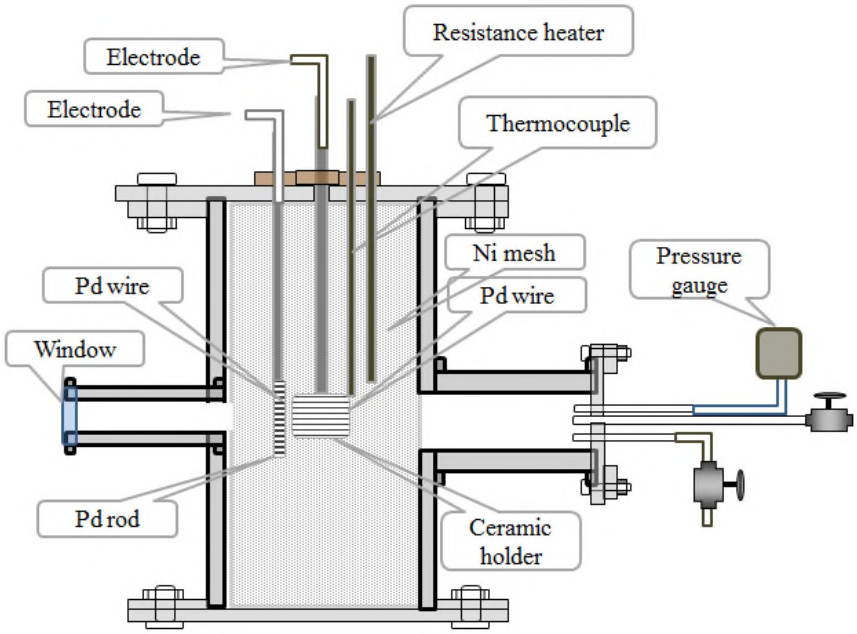


**Figure 10. Cross section of the large reactor.**

## Description of small reactor and electrodes

Figure 11 shows the small reactor, which is 400 mm tall, 114 mm diameter, made of SUS stainless steel. The volume is 2 L, weight 11 kg. The upper portion includes the electrode connections, the gas supply pipe and the vacuum exhaust pipe. A 6-mm diameter copper cooling tube is wound around the outer wall, to remove heat from the reactor. Calorimetry has not been performed with this cooling flow, but it may be in future tests.

The counter-electrode shown in this diagram is a nickel wire mesh at the bottom of the chamber. This is 0.05 mm diameter wire (50-mesh). (As noted above, there is another nickel mesh touching the walls of the reactor chamber, shown in Fig. 12.) The upper electrode is insulated with an alumina tube 6 mm in diameter. The structure of the electrode varied from one test to another, with electrodes in the form of plates, particles, wire or mesh. The lower counter-electrode was also varied, from plate, particles or mesh.

With the small reactor, high voltage positive current is supplied to the electrode in the middle of the cell. The counter electrode is at ground potential, because it touches the cell vessel wall, which is grounded. With this power supply, changing to negative voltage is inconvenient. With the large reactor, power is supplied to both electrodes and the polarity can be easily reversed.

Figure 12. The small reactor

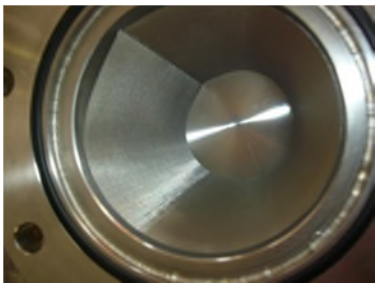

Figure 13. Small reactor inside view. A nickel mesh shields the wall from the plasma.

Figure 11. Small reactor electrode

Figure 14 shows a simplified cross section of the small reactor. The electrodes are about 200 mm apart. This schematic does not include the thermocouple or the resistance heater.

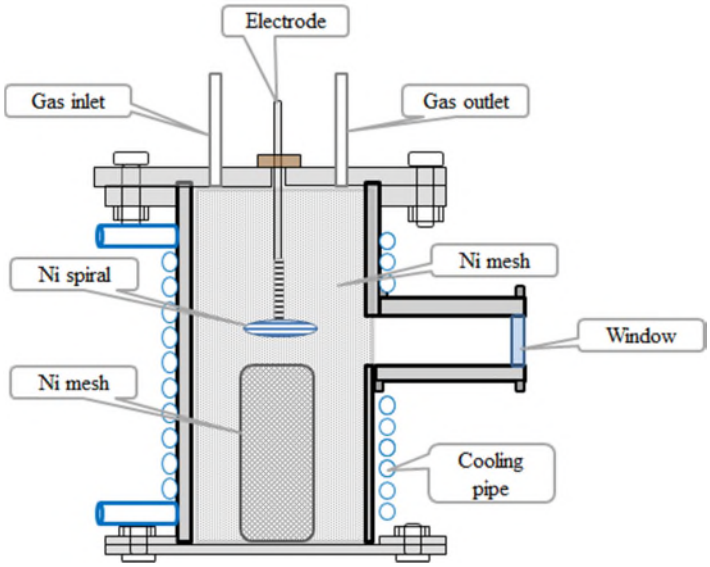


Figure 14. Small reactor cross section.

## 2.5 Equipment configuration

Figure 15 shows a block diagram of the reactor, the control system, the vacuum exhaust and mass spectroscopy system, and the measurement and control systems. Voltage is applied from the high voltage (HV) power supply (left side of diagram). Also shown on the left is the computer, data logger, power analyzer and waveform analyzer. Along the top of the cell is a neutron detector and gamma detector, and a pressure gauge. In this diagram, the cell is shown in the lower portion. On the right side is shown one of the two K-type thermocouples measuring the reactor vessel wall temperature (T5 is shown; T6, at the base, is not). Another thermocouple is inside the cell, in direct

contact with the electrode surface. The bottom right of the diagram shows the gas supply and quadrupole mass analyzer used to analyze the gas withdrawn from the cell. Temperature is measured in 4 locations total (including ambient temperature). Temperature, voltage, power, pressure, the neutron and gamma count, and the gas analysis is collected by the logger and recorded in the computer every few seconds.

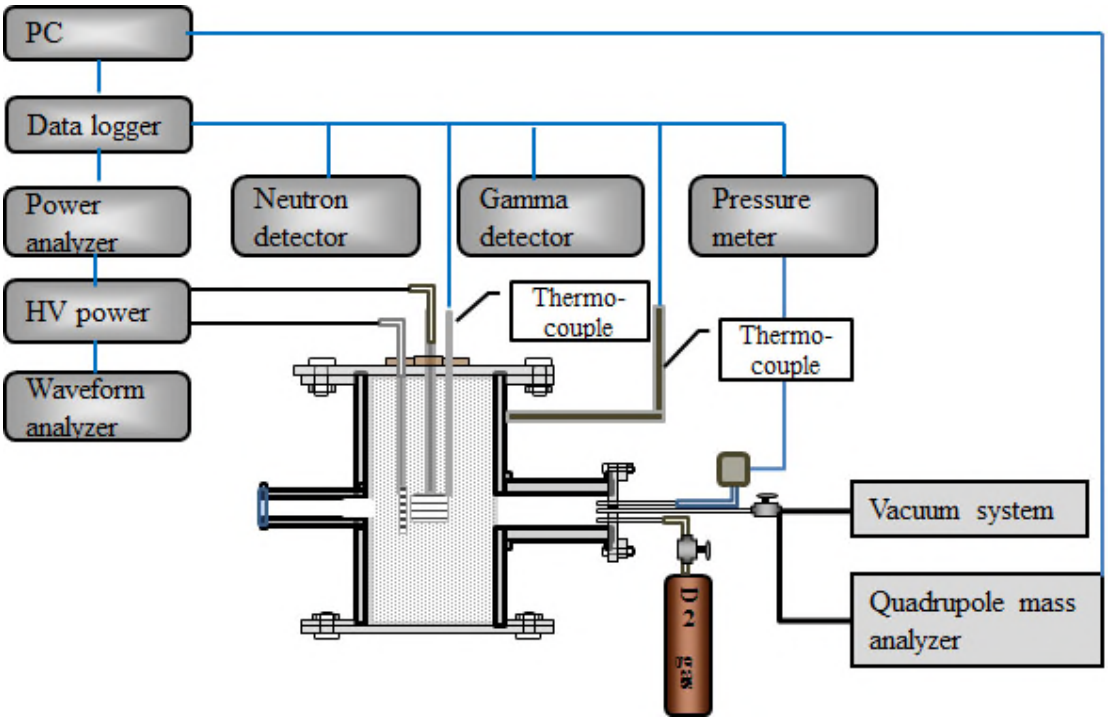


Figure 15. Equipment configuration.

# 3 Method of controlling heat

The method of controlling the anomalous heat is described for the large reactor. The electrodes are as shown in Fig. 9.

## 3.1 Vacuum

The reactor vessel is evacuated down to several Pascals.

## 3.2 Glow discharge to form nanoparticles

After evacuating the reactor, the gas level is held at several Pascals, and electrons from the central electrode are used to bombard the counter-electrode in the big reactor, or the reactant material placed against the bottom of the small reactor. This activation treatment step exposes the metal, cleaning off impurities and oxides. As shown in Fig. 15, voltage and current are applied to the electrodes. At first the 0.1 mm thin wire palladium mesh is made the positive electrode at 600 V, and glow discharge at 20 mA is continued for 600 s. Then the mesh is switched to negative terminal, and glow discharge continues for 1200 s, again at 600 V and 20 mA.

This glow discharge cycle is repeated for about 15 hours with the thin 0.1 mm diameter wire, or for 30 hours with the 1 mm wire. Glow discharge continues until many nanoparticles form on the surface, and the surface is activated.

## 3.3 Heat treatment

The vessel is then evacuated to a lower pressure while the electrodes are hot, to remove additional impurities. The electrodes are then activated by being heated with the resistance heater, to temperatures between 100°C and 200°C for about 3 hours. This continues until light hydrogen, $H_2O$, and gaseous hydrocarbons are driven out of the electrodes and are no longer detected by the mass spectrometer in significant levels.

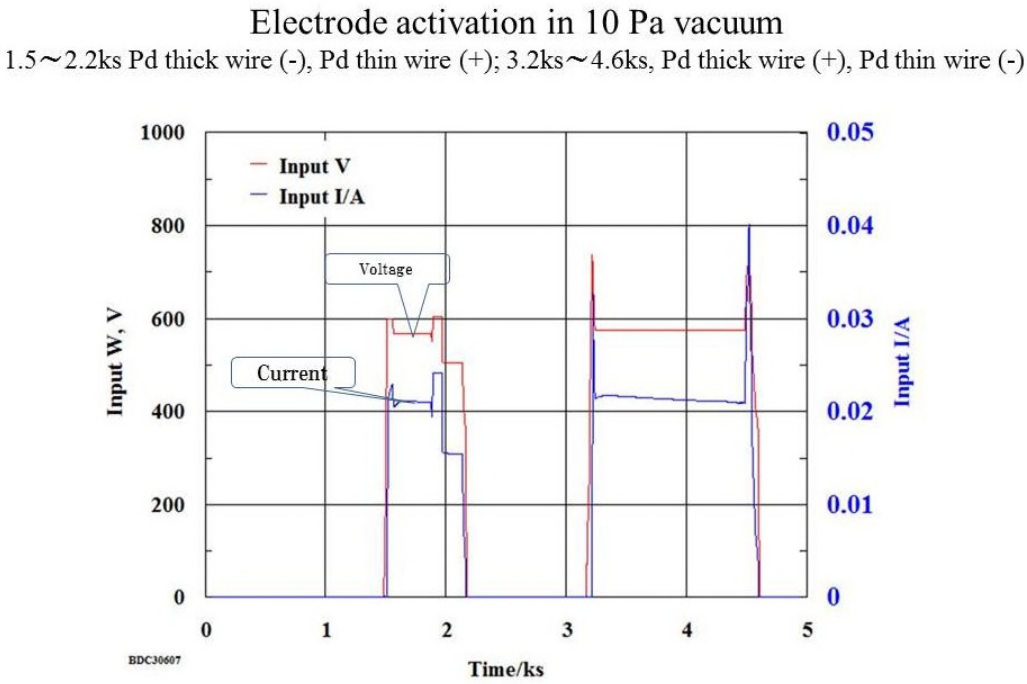


Figure 16. Electrode heating power input.

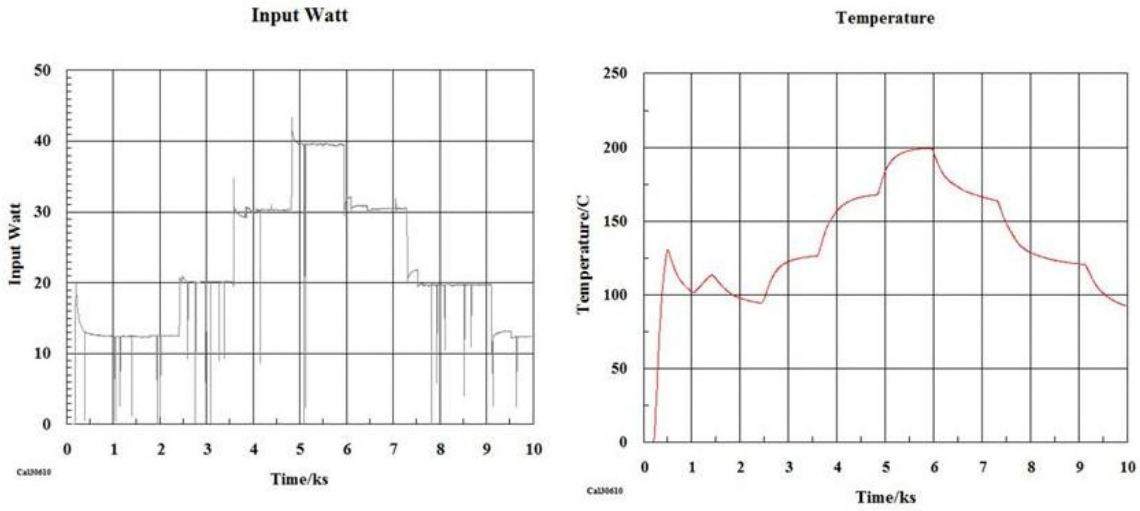


Figure 17. Temperature changes in the electrodes during heating.

## 3.4 Glow discharge heating

Glow discharge is then performed to produce nanoparticles on the electrode surface. The thin wire palladium electrode is the positive terminal. Direct current glow discharge is maintained at

about 20 ~ 30 mA and 600 to 800 V for about 10 ks (10 kiloseconds; ~27 hours). After this, $D_2$ gas is admitted into the cell, and it absorbs into the electrode surface. Figure 18 shows the resulting temperature changes. This figure shows the difference between the electrode temperature and ambient temperature. Figure 19 shows a SEM photo of the palladium wire electrode surface after this treatment, and Fig. 20 shows a nickel wire. Fine metal particles (nanoparticles) are formed on the metal surface. The magnification here is 2000 times, which is enough to reveal nanoparticles of less than 1 micrometer. When the SEM magnification is increased, even smaller particles can be seen. Particles on the nanometer scale are ideal.

This method produces nanoparticles *in situ* after cleaning and purifying the electrode material, in a high-purity gas environment. So the nanoparticles have little contamination on the surface and they are highly absorbent. With other methods, the nanoparticle material is fabricated elsewhere and exposed to air and contamination before being placed in the cell.

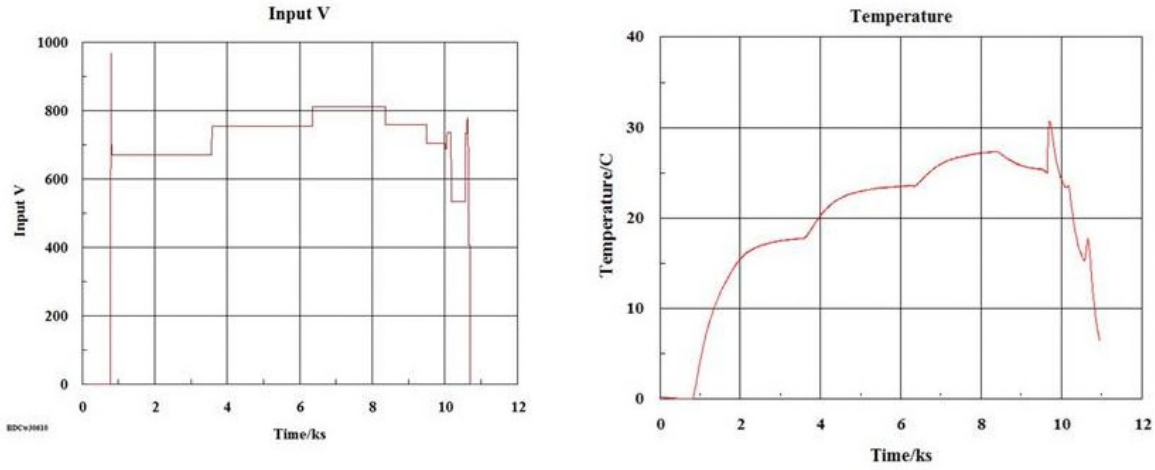


**Figure 18. Heat treatment with glow discharge.**

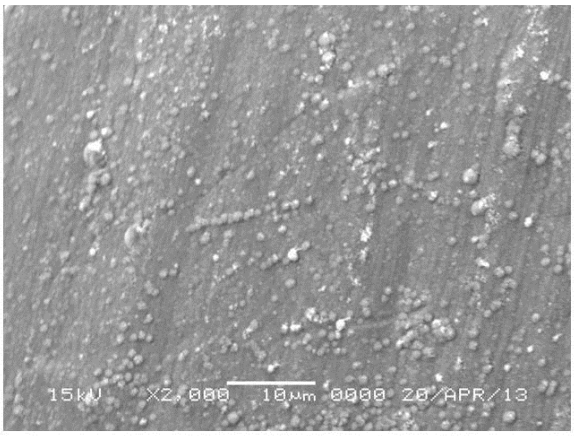


**Figure 19. SEM photo of palladium thin wire after treatment.**

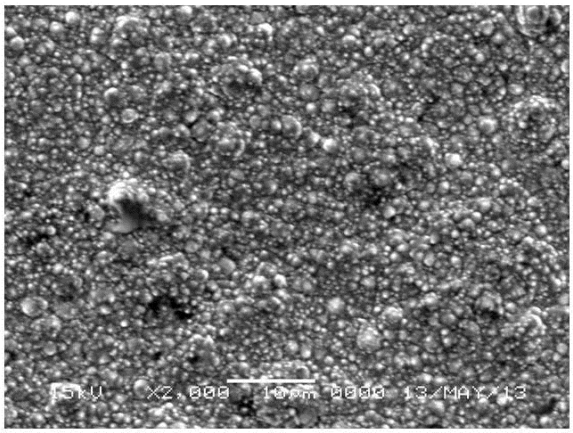


Figure 20. Nickel after activation treatment.

## 3.5 Anomalous exothermic reaction

The palladium thin wire is made the negative electrode in a vacuum. As shown in Fig. 21, it is subjected to glow discharge at 800 V for about 11 ks (3 hours), before changing the polarity to make it the positive electrode and continuing glow discharge. Input power is steady during these phases, at around 16 W.

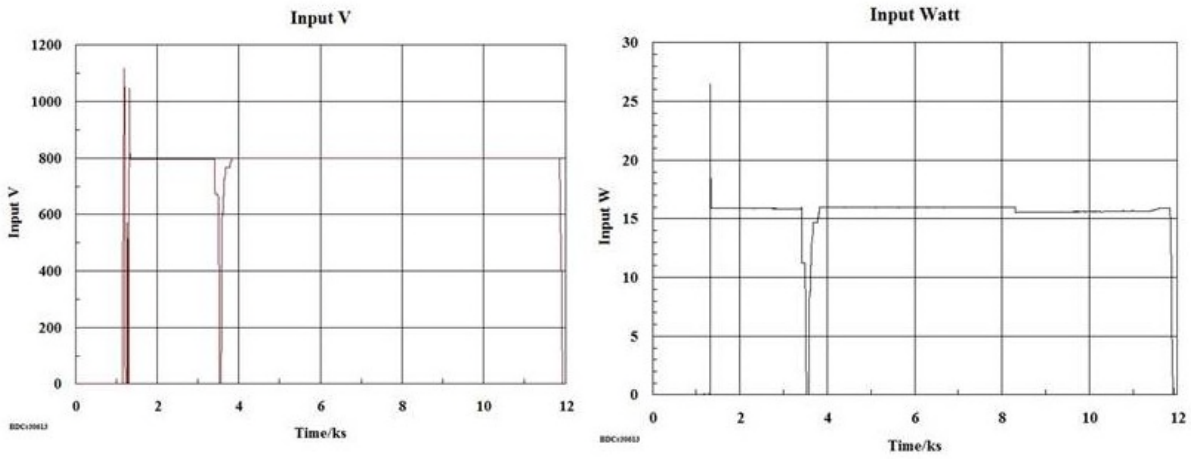


Figure 21. Changes in voltage during the anomalous exothermic reaction, and changes in input electric power.

# 4. Anomalous heat results

## 4.1 Resistance heater calibration

Before each glow discharge run the cell was calibrated with the resistance heater. The resistance heater is stepped through several power levels from 5 to 45 W. After about 3 hours at a given power level, the temperature stabilizes and temperature is recorded. The temperatures at the electrode surface are shown in Fig. 22. Data points for $D_2$ gas at 100 Pa and a vacuum at 10 Pa are shown. The response was nearly linear and very close for both gas and a vacuum.

This calibration curve demonstrates that the cell reliably and repeatedly reaches the same temperature at a given power level with resistance heating. However, the calibration for the electrode is not an accurate method to determine the power level during glow discharge. The temperature does not always correspond to the power level because the plasma transfers heat away from the electrode, and because of plasma instability. (Examples of this are shown below.)

The temperature at the cell wall (T5) and the base of the cell (T6) were also recorded, and these are the same for with resistance heating and glow discharge. In this paper, power out is calculated as a function of T5 and T6.

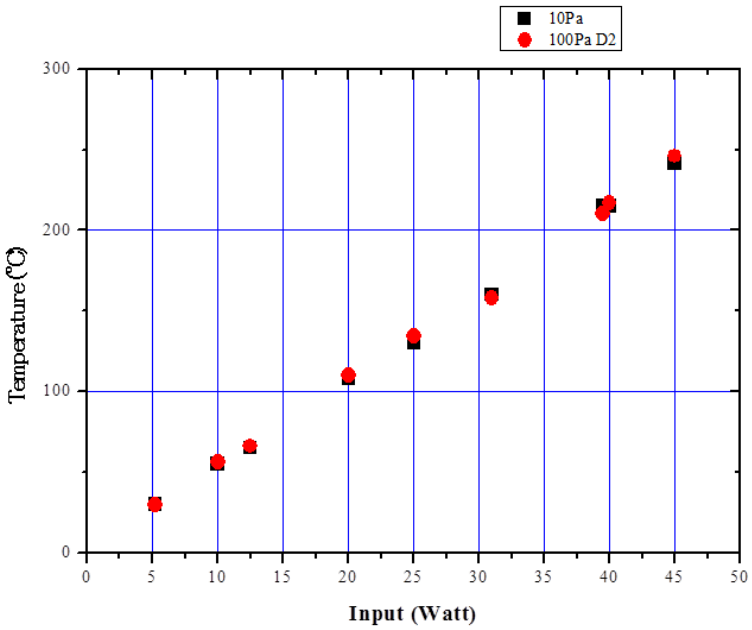


**Figure 22. Electrode temperatures during calibration with resistance heater. The black squares are a vacuum at 10 Pa and the red circles are $D_2$ gas at 100 Pa.**

## 4.2 An example of anomalous heat

An example of anomalous heat is shown in Fig. 23. During this event, 800 V, 20 mA was conducted between the electrodes. Total power was 16 W. Anomalous heat occurred when the palladium wire was the negative electrode. Initially, 34.3 kJ of energy was expended in glow discharge, and 4.4 kJ of anomalous excess heat was produced. When the electrode was switched to the positive terminal, the temperature, which had been in thermal equilibrium, again rose. During this time input power remained at 16 W, and the cell had reached thermal equilibrium, never rising more than 15°C above ambient. After 8.5 ks, the temperature rose and an additional 54 kJ of heat was detected. When an additional 10 ml of deuterium gas was added, raising the pressure 10 Pa, the anomalous heat momentarily rose again, producing an extra 15 kJ. This event continued for about 100 s, indicating a power level of about 150 W.

In some cases heat is produced when gas is added to the cell after glow discharge power is turned off, showing that the gas itself is the cause of the heat.

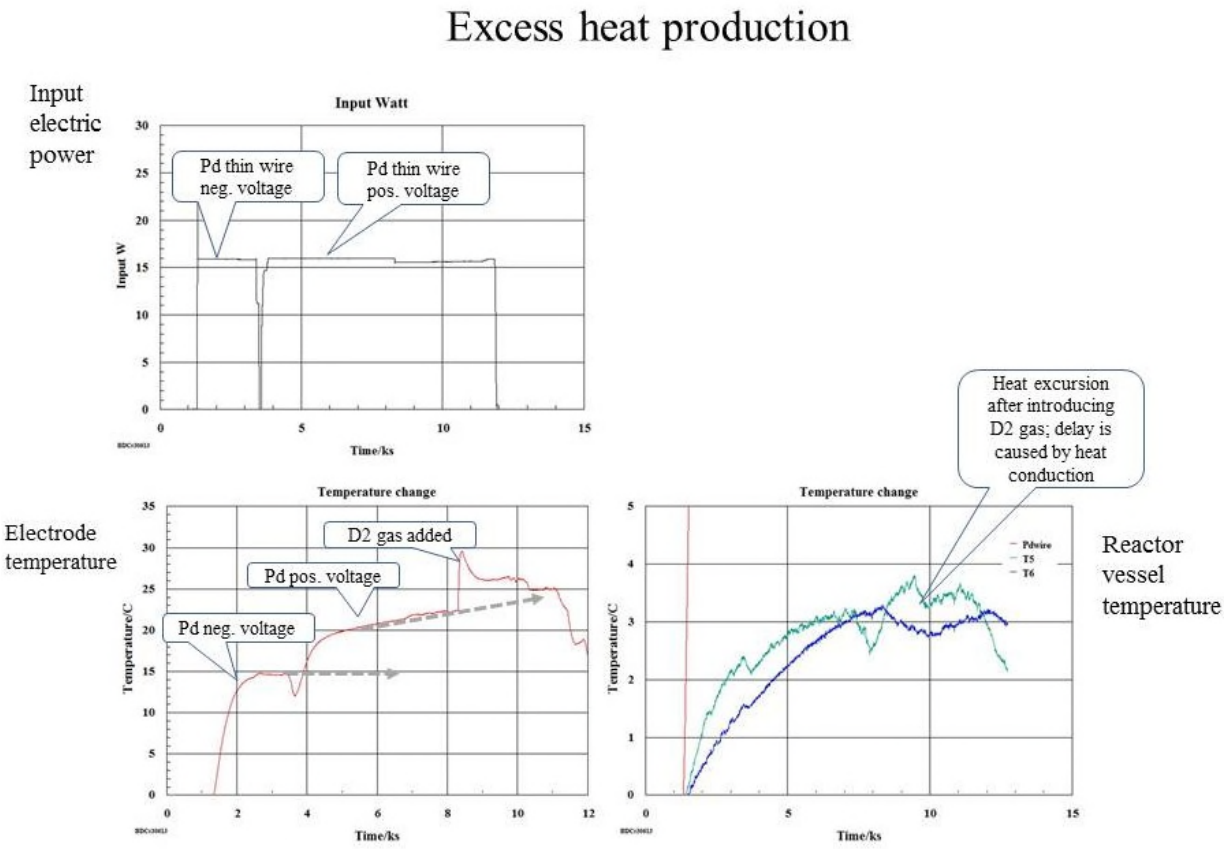


**Figure 23. Excess heat production details.**

As noted, although the cell calibration with a resistance heater is linear, stable and repeatable, the electrode temperature in response to glow discharge is not. The temperature is generally lower than with same power level of resistance heating. In some cases, even when glow discharge power is increased, the electrode temperature does not increase.

Figure 24 shows an example in which positive voltage glow discharge began at 13.9 ks. Glow discharge power was also increased from 33 to 49 W. Despite the increased power, the electrode temperature did not rise significantly. This is evidence that the plasma moves the heat from the electrode to other locations in the cell. Sensors T5 and T6 on the outside of the cell did detect the increased input power, plus they detected anomalous heat. At 17.2 ks, voltage was again negative, and the reactor wall temperature falls (sensor T5). The electrode temperature falls slightly. The wall temperature remains higher than it was from 0 to 17.2 ks, because glow discharge power is higher. But the anomalous excess heat component has gone.

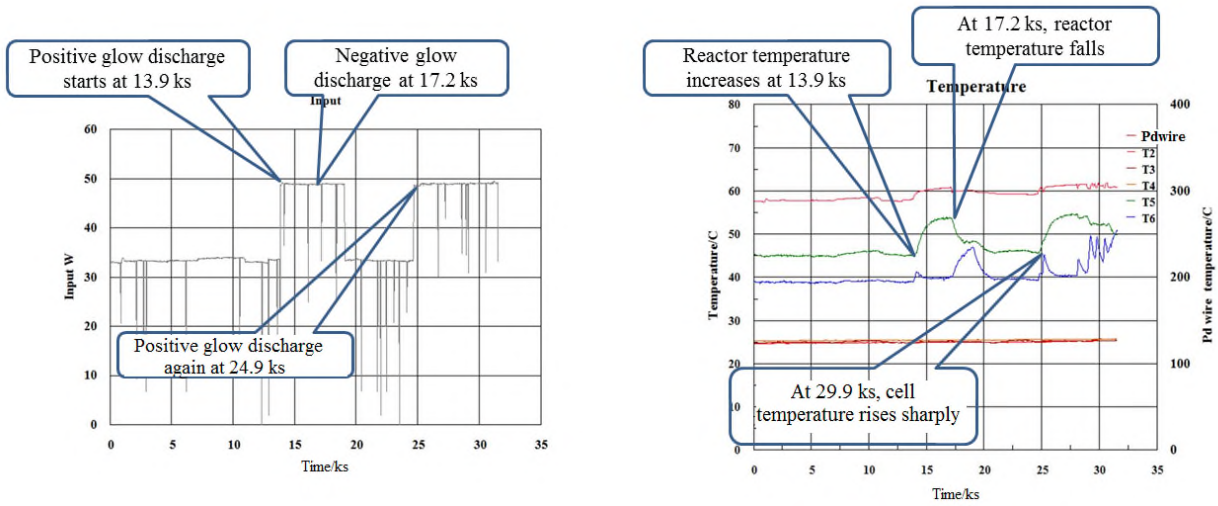


**Figure 24. D2 gas and glow discharge applied. Electrode temperature does not change much, but the cell wall temperature does.**

Figure 25 shows a portion of Fig. 24, in which the T5 sensor at the cell wall detects both glow discharge and anomalous cold fusion heat. In step 1, T5 is at 45°C. This is the baseline temperature for negative voltage glow discharge at 33 W. In step 2, glow discharge power is increased to 49 W, and polarity is reversed which triggers anomalous heat. T5 quickly rises to 54°C. In step 3, polarity is again reversed and the anomalous heat goes away. T5 falls to a level above baseline because glow discharge is still at 49 W. In step 4, glow discharge power is reduced back to the original 33 W, and T5 returns to the baseline temperature.

The Pdwire sensor rises and falls only slightly, because the plasma removes heat from the electrode.

The T6 sensor at the bottom of the cell lags behind Pdwire and T5. At the end of the run the entire reactor cylinder comes to the same temperature.

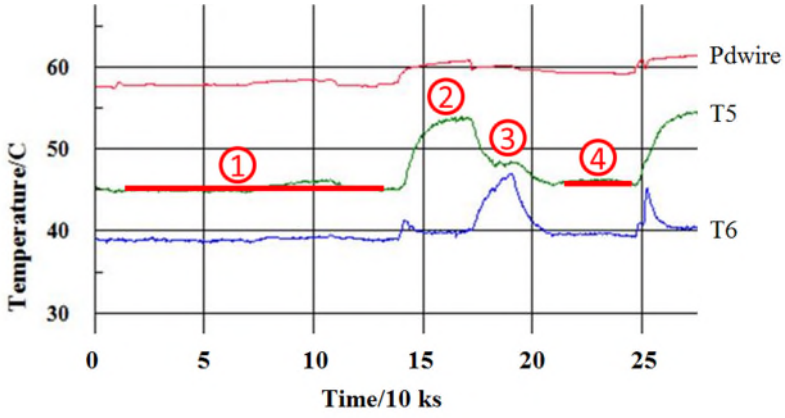


**Figure 25. A close up look at Fig. 24. The T5 thermocouple is shown: ① at baseline 33 W negative voltage glow discharge; ② 49 W positive glow discharge, with cold fusion anomalous heat; ③ 49 W negative glow discharge, no anomalous heat; ④ back to negative voltage 33 W (the baseline).**

In a recent test, the cell became very hot. The T5 thermocouple loosened and did not record the temperature correctly. An IR camera showed the surface temperature to be 80°C where the heater calibration showed it should not have exceeded 40°C.

Twenty-five out of 50 tests produced significant excess heat. During excess heat production, neutrons, gamma rays and x-rays were also observed in some cases. Data on this will be presented later. Table 1 shows a summary of the 25 successful tests. Electrodes were nickel or palladium. Electrodes in the shape of coils and spirals were wrapped around tubes. The gas was either a vacuum, hydrogen or deuterium gas. The tests were performed after both electrodes were activated with glow discharge for many hours. The electric power was either direct current or alternating current at 50 Hz. Voltage up to 1000 V was used.

In Table 1, “energy in” includes resistance heat and glow discharge. “Heat out” is calculated based of the temperatures of T5 and T6 during calibration with the resistance. The last column shows the ratio of excess heat and input power.

## Table 1. Summary of the 25 successful tests

| Test | Reactor | Electrode | | Gas | Pressure | Applied V | | Energy in/ kJ | Heat out/kJ | Out/in |
|---|---|---|---|---|---|---|---|---|---|---|
| | | Anode + | Cathode - | H2 or D2 | Pressure/Pa | Current | Volt | | | |
| 1 | **Small** | Ni wire coil | Ni mesh | H2 | 10 | DC | 605 | 17.9 | 27.0 | 1.51 |
| 2 | **Big** | Pd wire coil | Pt mesh | H2 | 10 | DC | 700 | 13.0 | 19.7 | 1.52 |
| 3 | **Small** | Ni wire coil | Ni mesh | H2 | 10 | AC | 1000 | 25.3 | 4.0 | 0.16 |
| 4 | **Big** | Pd wire coil | Pt mesh | D2 | 10 | DC | 800 | 30.3 | 45.6 | 1.50 |
| 5 | **Big** | Ni wire coil | Ni mesh | H2 | 10 | AC 50Hz | 700 | 32.7 | 38.0 | 1.16 |
| 6 | **Big** | Ni wire coil | Ni mesh | D2 | 10 | DC | 800 | 38.8 | 45.6 | 1.18 |
| 7 | **Big** | Ni wire coil | Ni mesh | D2 | 10 | DC | 800 | 17.1 | 30.4 | 1.78 |
| 8 | **Big** | Ni wire coil | Ni mesh | D2 | 10 | AC 50Hz | 700 | 15.9 | 11.8 | 0.74 |
| 9 | **Small** | Ni wire spiral | Ni plate | H2 | 10 | DC | 600 | 8.3 | 15.6 | 1.88 |
| 10 | **Small** | Ni wire spiral | Ni plate | H2 | 10 | AC 50Hz | 800 | 16.2 | 25.9 | 1.60 |
| 11 | **Small** | Ni wire spiral | Ni mesh | H2 | 10 | DC | 600 | 24.5 | 50.6 | 2.07 |
| 12 | **Small** | Ni wire spiral | Ni mesh | H2 | 10 | AC 50Hz | 750 | 76.7 | 62.3 | 0.81 |
| 13 | **Small** | Ni wire spiral | Ni mesh | D2 | 10 | DC | 600 | 109.0 | 126.6 | 1.16 |
| 14 | **Small** | Ni wire spiral | Ni mesh | D2 | 10 | DC | 750 | 91.6 | 146.0 | 1.59 |
| 15 | **Small** | Ni wire spiral | Ni mesh | D2 | 10 | DC | 700 | 110.0 | 162.0 | 1.47 |
| 16 | **Big** | Pd wire | Pd rod | H2 | 80 | DC | 590 | 4.6 | 8.0 | 1.75 |
| 17 | **Big** | Pd rod | Pd wire | H2 | 60 | DC | 595 | 10.7 | 10.3 | 0.96 |
| 18 | **Big** | Pd wire | Pd rod | H2 | 10 | DC | 800 | 125.0 | 122.0 | 0.97 |
| 19 | **Big** | Pd wire | Pd rod | H2 | 70 | DC | 800 | 34.3 | 53.2 | 1.55 |
| 20 | **Big** | Pd wire | Pd rod | H2 | 20 | DC | 800 | 74.8 | 107.2 | 1.43 |
| 21 | **Big** | Pd wire | Pd rod | D2 | 80 | DC | 800 | 56.0 | 66.5 | 1.19 |
| 22 | **Big** | Pd wire | Pd rod | H2 | 80 | DC | 759 | 15.0 | 41.8 | 2.79 |
| 23 | **Big** | Pd wire | Pd rod | H2 | 80 | DC | 780 | 137.0 | 147.0 | 1.07 |
| 24 | **Big** | Pd rod | Pd wire | H2 | 80 | DC | 790 | 173.5 | 152.0 | 0.87 |
| 25 | **Big** | Pd rod | Pd wire | H2 | 80 | DC | 790 | 0.8 | 1.9 | 2.49 |

## Addendum

This preprint paper was presented at a poster session at ICCF18 in July 2013. After the conference, the author improved the calorimetry and ran a new series of tests. The problem described above in section 4.2, in which the Pdwire sensor rises and falls only slightly in response to excess heat, has now been address. Figure 26 shows the response of Pdwire (labeled “electrode” here) and the two outside wall sensors in the new configuration. The linear series of red data points are from calibration runs. They show that the electrode sensor registers ~260°C with 50 W input.

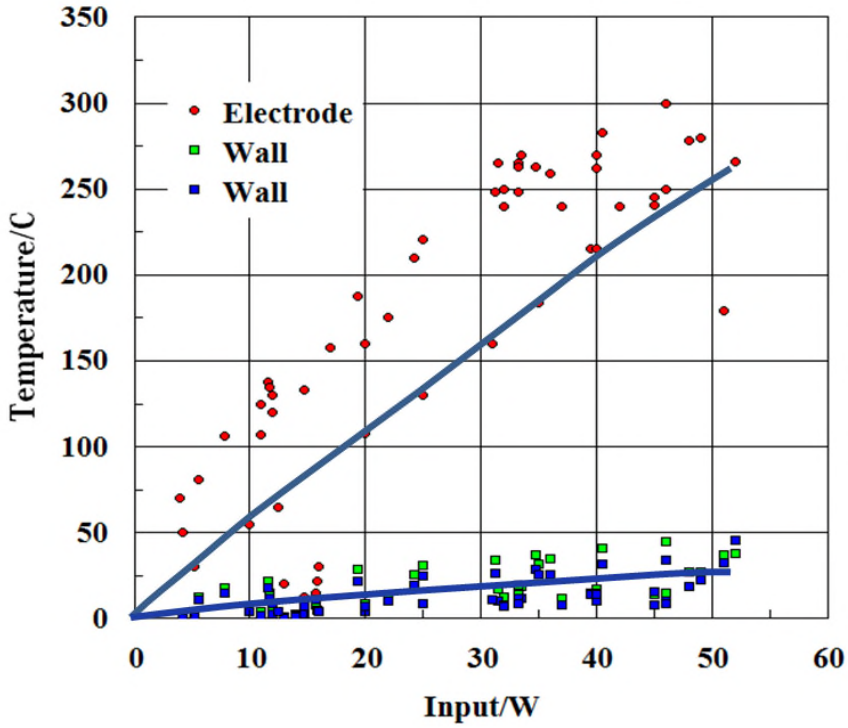


**Figure 26. Improved calorimeter temperature sensor response. The sensor labeled "electrode" was labeled "Pdwire" in earlier figures.**

Table 2 shows 22 additional tests performed with the improved calorimetry. Sixteen of these tests produced excess heat.

**Table 2. Twenty-two additional tests with improved calorimetry in the large reactor with palladium electrodes**

| Electrode | | Gas | | Applied V | | Power in/W | | Heat out/W | | Time/ ks | $H_{out}/H_{in}$ | | Temp./C | |
|---|---|---|---|---|---|---|---|---|---|---|---|---|---|---|
| Anode + | Cathode - | Component | Pressure/Pa | Heater/W | Plasma/V | Heater input | Plasma input | By electrode temp. | By reactor temp. | | By Electrode temp. | By reactor temp. | Electrode | Reactor |
| Rod | Wire | $D_2O$ | 70 | 30.7 | 0 | 30.7 | 0 | 51 | 34 | 7 | 1.65 | 1.08 | 240 | 43 |
| Rod | Wire | $D_2O$ | 70 | 30.7 | 780 | 30.7 | 13.9 | 61 | 48 | 2.8 | 1.37 | 1.08 | 260 | 60 |
| Rod | Wire | $D_2O$ | 275 | 31 | 0 | 31 | 0 | 58 | 35 | 58 | 1.87 | 1.13 | 260 | 55 |
| Rod | Wire | $D_2O$ | 50 | 31 | 0 | 31 | 0 | 46 | 34 | 78.3 | 1.48 | 1.07 | 200 | 52 |
| Rod | Wire | $D_2O$ | 50 | 31 | 0 | 31 | 0 | 43 | 31 | 12.8 | 1.38 | 1.00 | 210 | 47 |
| | | $D_2O$ | 100 | 45.7 | 0 | 45.7 | 0 | 53 | 55 | 64.7 | 1.15 | 1.19 | 275 | 51 |
| | | $D_2O$ | 20 | 44.6 | 0 | 44.6 | 0 | 36 | 50 | 1.2 | 0.82 | 1.13 | 190 | 50 |
| Wire | Rod | $D_2O$ | 50 | 45.8 | 790 | 45.8 | 16.6 | 62 | 62 | 2.48 | 0.99 | 1.2 | 320 | 70 |
| Rod | Wire | $D_2O$ | 50 | 46.6 | 772 | 46.6 | 14.6 | 60.4 | 60 | 1.44 | 0.99 | 1.3 | 320 | 70 |
| | | $D_2O$ | 50 | 47 | 0 | 47 | 0 | 55 | 55 | 1.17 | 1.28 | 1.43 | 315 | 64 |
| Rod | Wire | $D_2O$ | 145 | 45.9 | 0 | 45.9 | | 124 | 114 | 75.2 | 2.7 | 2.48 | 280 | 65 |
| Rod | Wire | $D_2$ | 330 | 45.8 | 0 | 45.8 | | 64 | 63 | 62.5 | 1.4 | 1.37 | 325 | 64 |
| Rod | Wire | $H_2O$ | 20 | 46 | 0 | 46 | 0 | 46 | 70 | 8.2 | 1 | 1.09 | 250 | 60 |
| Wire | Rod | $D_2$ | 400 | 49 | 770 | 49 | 12 | 66 | 70 | 6.5 | 1.08 | 1.15 | 330 | 68 |
| | | $D_2$ | 200 | 49 | 0 | 49 | 0 | 61 | 60 | 1.3 | 1.24 | 1.22 | 300 | 63 |
| | | $D_2$ | 300 | 25 | 0 | 25 | 0 | 41 | 30 | 6.5 | 1.64 | 1.2 | 250 | 48 |
| Wire | Rod | D2 | 300 | 36 | 0 | 36 | 0 | 54 | 48 | 1.5 | 1.5 | 1.33 | 300 | 55 |
| | | D2 | 330 | 36 | 0 | 36 | 0 | 54 | 44 | 2.8 | 1.5 | 1.22 | 285 | 55 |
| | | D2 | 330 | 51.2 | 0 | 51.2 | 0 | 58 | 80 | 8 | 1.13 | 1.56 | 298 | 70 |
| | | $H_2O$ | 20 | 35.5 | 0 | 35.5 | 0 | 42 | 42 | 60 | 1.18 | 1.18 | 230 | 55 |
| Rod | Wire | $H_2O$ | 150 | 15.6 | 825 | 0 | 15.6 | 4.3 | 10 | 16 | 0.28 | 0.66 | 45 | 33 |
| Wire | Rod | $H_2O$ | 145 | 16 | 800 | 0 | 16 | 3.1 | 10 | 9.4 | 0.19 | 0.66 | 44 | 35 |

## References


1. Tadahiko Mizuno, Tadashi Akimoto and Norio Sato, “Neutron Evolution from Annealed Palladium Cathode in LiOD-$D_2O$ Solution”, The Electrochemical Society of Japan, Vol.57, No.7, (1989) 742-743, in Japanese.
2. Tadahiko Mizuno, Tadashi Akimoto, Kazuhisa Azumi and Norio Sato, “Tritium evolution during cathodic polarization of palladium electrode in $D_2O$ solution”, The Electrochemical Society of Japan Vol.59, No.9, (1991) 798-799. in Japanese.
3. Tadahiko Mizuno and Michio Enyo, “Hydrogen Absorption and Hydride Formation in Ti During Cathodic Electrolysis” Denki Kagaku, 63, 8, (1995) 719-725, in Japanese.
4. Tadahiko Mizuno, Tadayoshi Ohmori, Kazuya Kurokawa, Tadashi Akimoto, Masatoshi Kitaichi, Koichi Inoda, Kazuhisa Azumi, Shigezo Shimokawa and Michio Enyo, “Anomalous Isotopic Distribution of Elements Deposited on Palladium Induced by Cathodic Electrolysis” Denki Kagaku, 64, 11, (1996) 1160-1165, in Japanese.
5. Tadahiko Mizuno, Tadashi Akimoto, Tadayoshi Ohmori, Akito Takahashi, Hiroshi Yamada and Hiroo Numata, “Neutron Evolution from a Palladium Electrode by Alternate Absorption Treatment of Deuterium and Hydrogen” Jpn. J. Appl. Phys, Vol. 40 (2001) L989-L991
6. Tadahiko Mizuno, Tadashi Akimoto, Kazuhisa Azumi, Tadayoshi Ohmori, Yoshiaki Aoki, Akito Takahashi, “Hydrogen Evolution by Plasma Electrolysis in Aqueous Solution”, Jpn. J. Appl. Phys., Vol. 44, No. 1A (2005) 396-401.
7. Tadahiko Mizuno, “Transmutation Reaction in Condensed Matter”, Low-Energy Nuclear Reactions Sourcebook, American Chemical Society symposium series 998, 2008 271-294, ed. Jan Marwan and Steven B. Krivit.